Journal of Building Engineering 47 (2022) 103816

Contents lists available at ScienceDirect

Journal of Building Engineering

journal homepage: www.elsevier.com/locate/jobe

Effects of exposure temperature on the piezoresistive sensing performances of MWCNT-embedded cementitious sensor

Daeik Jang [a], H.N. Yoon [a], Joonho Seo [a], Beomjoo Yang [b, *]

[a] Department of Civil and Environmental Engineering, Korea Advanced Institute of Science and Technology (KAIST), 291 Daehak-ro, Yuseong-gu, Daejeon, 34141, Republic of Korea

[b] School of Civil Engineering, Chungbuk National University, 1 Chungdae-ro, Seowon-gu, Cheongju, Chungbuk, 28644, Republic of Korea

ARTICLE INFO

Keywords:
Multi-walled carbon nanotube (MWCNT)
Exposure temperatures
Cement-based sensors
Electrical characteristics
Piezoresistive sensors

ABSTRACT

Cement-based sensors are vulnerable to weathering conditions, such as exposure temperatures and freeze-thaw cycles, which have detrimental effects on their piezoresistive sensing behaviors; however, to the best of our knowledge, these effects have been rarely investigated. In this study, the electrical and piezoresistive sensing characteristics of multi-walled carbon nanotube (MWCNT)-embedded cement-based sensors exposed to various temperatures were investigated. Cement-based sensors with varying MWCNT content were fabricated and exposed to five different temperatures. Subsequently, the effects of these temperatures on the compressive strength and electrical properties of the sensors were observed. In addition, the electrical stability of the tunneling-induced and temperature-dependent electrical properties were examined. The electrical and piezoresistive sensing behaviors were found to be mainly affected by the exposure temperature, and the effects varied with the embedded MWCNT content. Thermo-gravimetric and scanning electron microscopy analyses served to characterize the microstructures of the cement-based sensors and the results helped in explaining the electrical and piezoresistive sensing behaviors.

1. Introduction

The accelerated advancement of electrically conductive cementitious composites is essential for satisfying the requirements of various applications (e.g., structural health monitoring sensors, electrical-heating composites, and electromagnetic wave shielding composites) [1–5]. To design conductive cementitious composites, carbon nanotubes (CNTs) have been widely used as a potential electrically conductive filler capable of forming electrically conductive networks in cementitious composites owing to their high electrical conductivity [5–8]. Many studies have reported that the piezoresistive sensing properties of CNT-embedded cement-based sensors are such that the electrical resistance changes when external force is applied [9–11]. Zhang et al. fabricated electrostatic self-assembled cementitious sensors by incorporating 0.5 vol% of CNT, which exhibited a stress sensitivity of 0.4% MPa^{-1} [9]. Naeem et al. investigated the possibility of CNT-embedded cement-based sensors as crack sensors; these types of composites demonstrated a 6.0% fractional change in the electrical resistance under 1.2 MPa of flexural stress [10].

Recently, the effects of weathering conditions such as the moisture content, water ingress, and elevated exposure temperature were assessed to observe the sensing stability of cement-based sensors [12–15]. Kim et al. observed the effects of moisture content on the piezoresistive sensing properties of cementitious composites; they reported that the stability of piezoresistivity improved as the

* Corresponding author.
E-mail address: byang@chungbuk.ac.kr (B. Yang).

https://doi.org/10.1016/j.jobe.2021.103816
Received 9 November 2021; Received in revised form 2 December 2021; Accepted 3 December 2021
Available online 9 December 2021

Table 1
Composition of cement-based sensors with various MWCNT content (wt.%).

SensorCode	w/b[a]	Cement	Silica fume	MWCNT	PSS	Nylon fiber	Water	SP
C2	0.5	100	5	0.2	0.2	0.1	52.5	0.8
C5		100	5	0.5	0.5	0.1	52.5	0.8
C10		100	5	1.0	1.0	0.1	52.5	0.8

[a] w/b denotes the water-to-binder ratio.

Table 2
Composition of the solutions used in zeta potential measurement.

Solution	Water	MWCNT	PSS
Water with MWCNT	40 mL	0.01 g	0.00 g
Water with PSS	40 mL	0.00 g	0.01 g
Water with MWCNT and PSS	40 mL	0.01 g	0.01 g

moisture content decreased [12]. Dong et al. investigated the physicochemical and piezoresistive properties of cementitious composites incorporating CNT when exposed to elevated temperatures; they found that the hydration products of heat-treated composites decomposed, which led to changes in the piezoresistive properties of the cementitious composites [14]. In addition, Jang et al. reported that the electrical properties and piezoresistive sensing performance of CNT-incorporated cementitious composites are mainly affected by water ingress, which possibly degrades their sensing capability [15]. Furthermore, many researchers have developed the conductivity model for predicting the electrical conductivity and sensing performances of the cement-based sensors. Kim et al. [16] and Lee et al. [17] proposed the conductivity model and parametric model for CNT/cement sensors, and the effects of crack on conductivity of sensors and the causes of fluctuation of electrical conductivity of the sensors were investigated, respectively. Tafesse et al. [18] developed mathematic-based intuitive model for accessing the effects of CNT dispersion on the conductivity of cement-based sensors. In addition, García-Macías et al. [19] proposed the lumped circuit for cement-based sensor as they were compressed under the dynamic loadings, and Sun et al. [20] also proposed the equivalent circuit for cementitious sensors under the different environmental conditions. Meanwhile, several studies have investigated the piezoresistive sensing response of cement-based sensors to advance their possible applications and assess the effects of certain weathering conditions on the piezoresistive sensing properties of these sensors. Nevertheless, fewer efforts have been made to investigate the electrical stability and piezoresistivity performances of the cement-based sensors with different CNT-embedded content when exposed to various exposure temperatures (e.g., elevated temperatures and freeze-thaw conditions) subjected to dynamic loading conditions.

Therefore, in this study, the electrical stability and dynamic piezoresistive sensing performance of cement-based sensors when exposed to various temperatures were investigated. Three different multi-walled CNT (MWCNT) content levels considering the percolation threshold of MWCNT-embedded cementitious composites and polysodium 4-styrenesulfonate (PSS) with equivalent MWCNT content (0.2, 0.5, and 1.0% by cement mass) were added to cementitious composites; subsequently, the fabricated composites were exposed to five different conditions (25, 100, 200, and 400 °C, and freeze-thaw cycling) after curing for 28 days. Under the static condition, the electrical resistance and electrical stability of the fabricated cement-based sensors exposed to different temperature conditions were observed. The temperature-dependent electrical properties of the sensors were examined when they were exposed to cyclic freeze-thaw conditions. In addition, the piezoresistive sensing performance of the sensors in dynamic loading conditions were investigated. The test results were characterized in terms of the maximum values of the fractional change in resistance (FCR) and gauge factors (GFs). Moreover, thermogravimetric (TG) and scanning electron microscopy (SEM) analyses were conducted to facilitate deep discussions of the electrical and piezoresistive sensing test results.

2. Experimental method

2.1. Fabrication of cement-based sensors

Ordinary Portland cement and silica fume, purchased from Elkem Inc. (EMS-970), were used as binder materials conforming to the ASTM C150 specification; additionally, multi-walled CNTs (MWCNTs, Jeio Co. Ltd., Korea) were added to the composites as an electrically conductive filler. The corresponding MWCNT diameter was 10 nm and the length ranged from 100 to 200 μ m. A polycarboxylate acid-type superplasticizer (Dongnam Co., Ltd., FLOWMIX 3000L) and PSS were added to the mixtures to homogenously disperse the MWCNT particles in the cement-based composites [7]. Nylon fibers (Nycon Fiber Inc., NYMAX) with diameters ranging from 23 to 36 μ m and a length of 3 mm were added to prevent shrinkage-induced cracks in the fabricated composites, and microcracks can be formed in the piezoresistive sensing tests. Three different amounts of MWCNT (0.2, 0.5, and 1.0% by cement mass) were added considering the percolation threshold range, and the same amounts of PSS as MWCNT were incorporated for MWCNT dispersion. The water-to-binder ratio was fixed at 0.5; moreover, 5% silica fume, 0.8% of a polycarboxylate acid-type superplasticizer, and 0.1% nylon fiber by cement mass were incorporated into the specimens. The details of the mix proportions used in this study are summarized in Table 1.

According to the previous studies [21,22], an incorporation of silica fume can increase the distances between the individual MWCNT particles due to the ball-bearing effect, and it may improve the dispersion of MWCNTs in the composites. It is also reported that

Table 3
Zeta potential values of the MWCNT and PSS in water.

Zeta potential (mV)	Water	Water with MWCNT	Water with PSS	Water with MWCNT and PSS
Absolute values	−16.90	−10.43	−26.55	−21.22
Relative values	0.0	6.47	−9.65	−4.32

the polycarboxylate-typed superplasticizer can enhance the CNT dispersion state due to the steric repulsion effect [22]. Furthermore, the utilization of poly (sodium 4-styrenesulfonate) (PSS) helps to disperse the MWCNT particles in the cementitious matrix [15]. Therefore, in the present study, the utilization of silica fume, superplasticizer, and PSS can contribute to improve the dispersion of MWCNTs in the cementitious composites. The cement-based sensors were fabricated as follows: the dry materials (in this case, OPC, silica fume, MWCNT, PSS, and nylon fibers) were put into a Hobart mixer; then, they were dried mixed for 5 min. The water and superplasticizer solutions were then introduced into the dried mixtures; they were mixed for an additional 5 min. The overall mixtures were then poured into 50 × 50 × 50 mm^3 cubical molds conforming to ASTM C109 [23]. Copper electrodes were embedded in the composites to measure the electrical properties, as reported in previous studies [15]. The composites were placed at an oven with room temperature (25 ± 2 °C) for 24h; subsequently, they were demolded and cured in an oven at room temperature for 27 days. Next, the fabricated cement-based sensors were dried in a 60 °C oven for additional 3 days to evaporate the moisture from the fabricated composites [11]. The sensors were then exposed to different temperature conditions (25, 100, 200, and 400 °C, and freeze-thaw cycles) for 1 h and they were assessed in terms of their compressive strength, electrical resistance, and piezoresistive sensing performance.

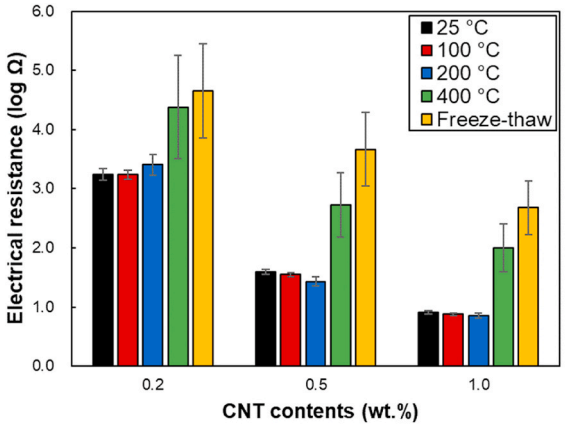

(a)

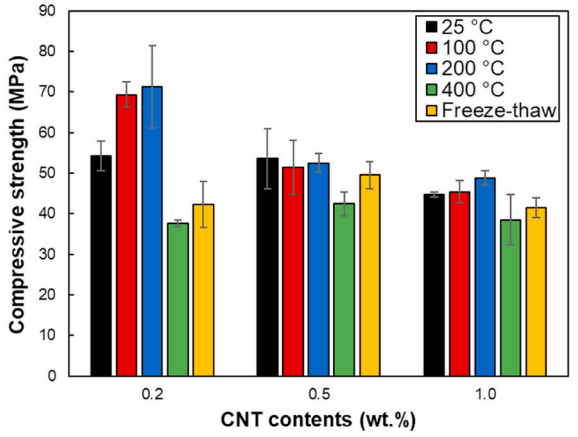

(b)

Fig. 1. (a) Electrical resistance and (b) compressive strength of specimens exposed to various temperatures.

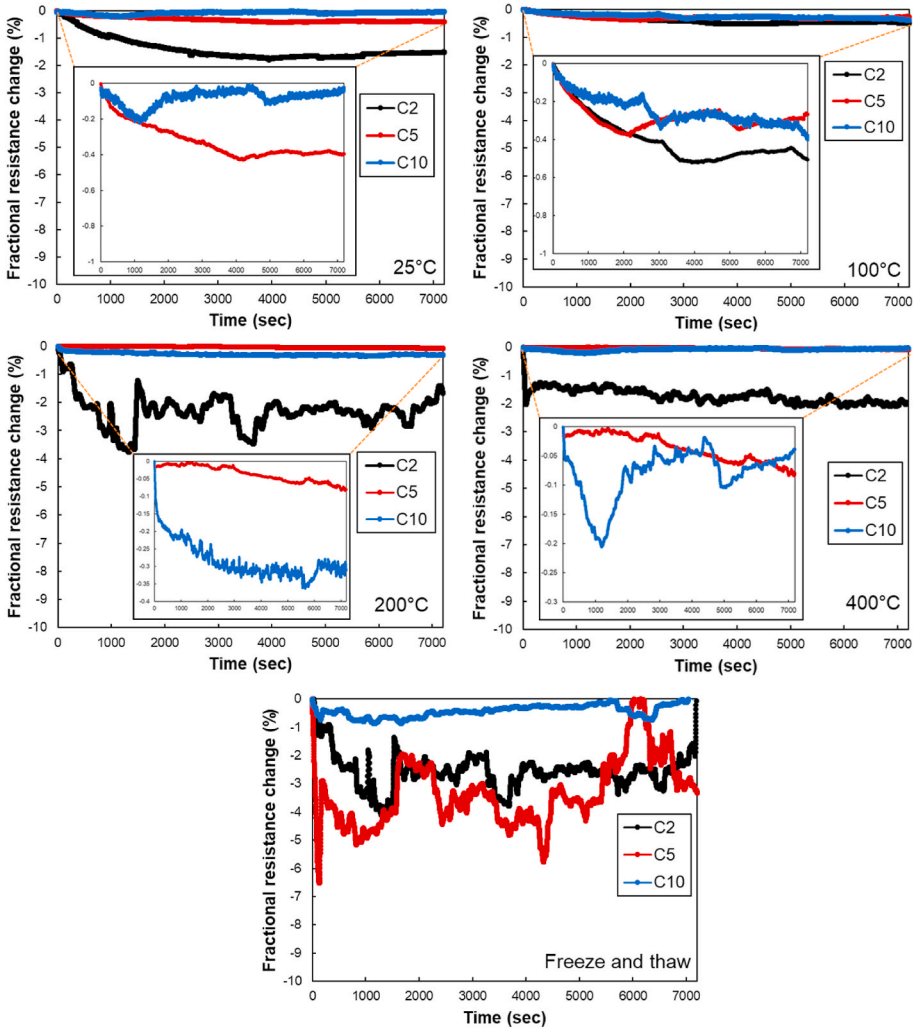

Fig. 2. Tunneling-induced electrical resistance of specimens in a static condition.

2.2. Experiment details

The dispersion characteristics of the MWCNT and PSS used in this study were evaluated via zeta potential tests [22]; water was used as the solvent to disperse them. Details regarding the mix proportions utilized in these tests are summarized in Table 2. An ultrasonicator (40 kHz; 200 W) was used to sonicate the solutions, including MWCNT, PSS, and water, for 1 h and the zeta potential values of the sonicated solutions were measured using a zeta potential analyzer (ELSZ-2000, Otsukael). The compressive strength was measured using a 2500 kN compression testing machine (INSTRON) with a constant loading rate of 0.02 mm/s, conforming to ASTM C 109. The electrical resistance values were measured using a digital multi-meter via the two-probe method [5,24,25]. Three replications were selected for each mix proportion to calculate the average values in both the compressive strength and electrical resistance measurement tests. The tunneling-induced electrical stability of the specimens was investigated in accordance with the previous studies by Jang et al. [7] and Park et al. [25]. A digital multi-meter (Agilent Tech, 34410A) was used to measure the electrical resistances of the specimens. Each probe was connected to the specimen and their electrical resistances were measured for 2h in the static condition without any applying loads. The measured electrical resistances were converted to fractional resistance change considering the initial electrical resistance value, which can indicate the electrical stability for 2 h [26–28]. To establish the temperature-dependent electrical properties, the specimens were put in a programmable chamber (EN-TH-1370) where the temperature was controlled from −15 to +15 °C for 50 cycles. Thus, the electrical resistance of the specimens was examined during freeze-thaw cycles. Meanwhile, the piezoresistive sensing performance of the cement-based sensors were investigated using a multipurpose servo-hydraulic universal testing machine (Walter Bai) with a load control method. The sensing behaviors of these sensors were investigated in two different dynamic conditions (i.e., short- and long-term loading conditions). In the short-term loading condition, cyclic triangular loadings with a frequency of 0.5 Hz were applied to the cement-based sensors from 0.5 to 25 kN for 10 cycles to investigate the sensitivity of the sensing performance considering the FCR. In the long-term loading condition, the identical loadings with a frequency of 2.0 Hz were applied to the sensors for 10,000 cycles to observe the sensing stability of the sensors. Meanwhile, the electrical resistance val-

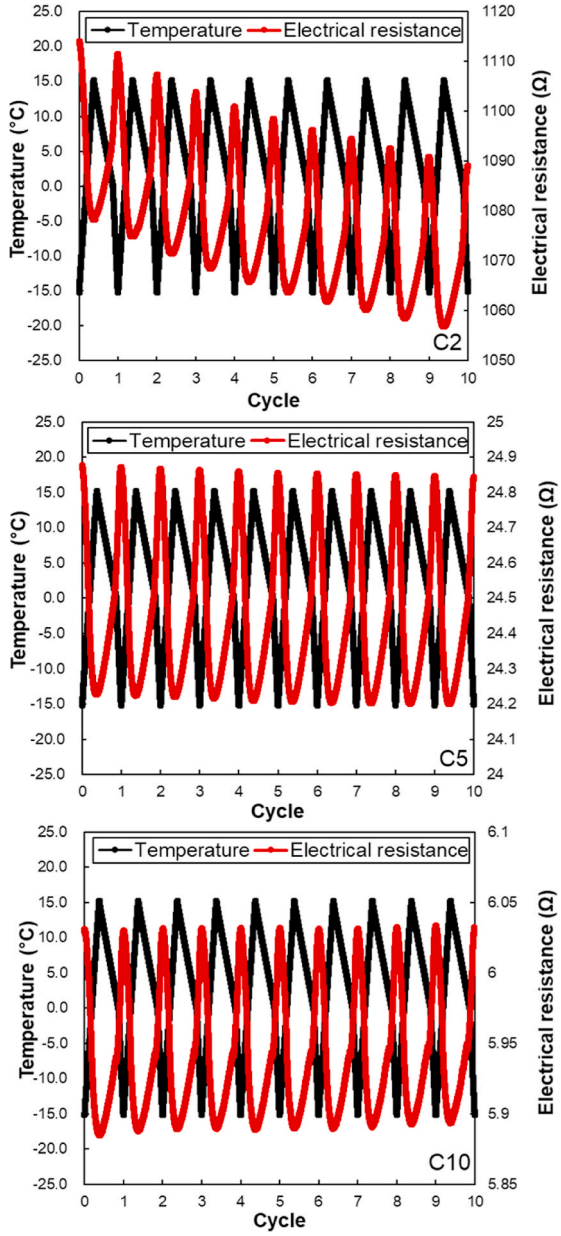

Fig. 3. Temperature-dependent electrical resistance of specimens during freeze-thaw cyclic tests.

ues of the sensors were measured. Then, the measured electrical resistance of the sensors was converted into the FCR and GF to evaluate the piezoresistive sensing performance of the cement-based sensors.

Microstructural images of the prepared fractured specimens, conforming to the RILEM recommendations, were captured via field emission-SEM (FE-SEM, Hitachi S4800) [29]. The fractured specimens exposed to various temperatures were immersed in isopropyl alcohol for 15 min; then, they were rinsed with isopropyl alcohol and vacuum filtered. Subsequently, they were stored in a vacuum desiccator before SEM analysis [30]. In addition, these specimens were manually ground to pass a 75 μ m sieve; 5.0–6.0 mg of this powder was used for TG-derivative thermogravimetry (DTG) analysis using a Labsys Evo TG-DTG instrument (SETARAM) in a temperature range of 25–1000 °C [23].

3. Results and discussions

It is noted that the mechanisms on the effects of elevated temperature and freeze-thaw cycles on the micro-structural changes in cementitious composites are different. Elevated temperature can lead to both decomposition of hydrates and the evaporation of residual moisture in the cementitious composites [14]. Meanwhile, the freeze-thaw cycle can cause microcracks due to the freezing and

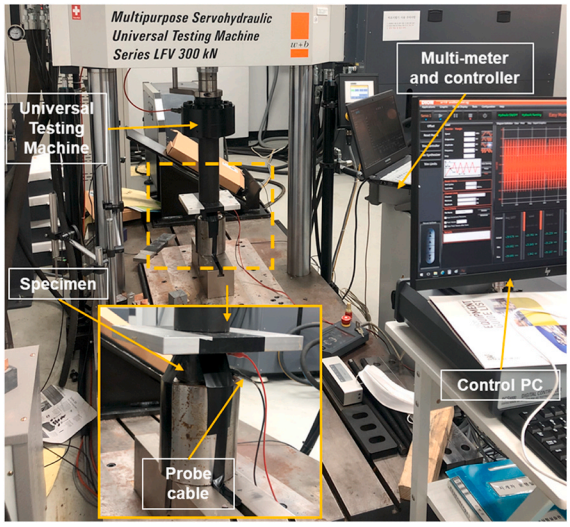

Fig. 4. Experimental setup for the piezoresistive sensing test.

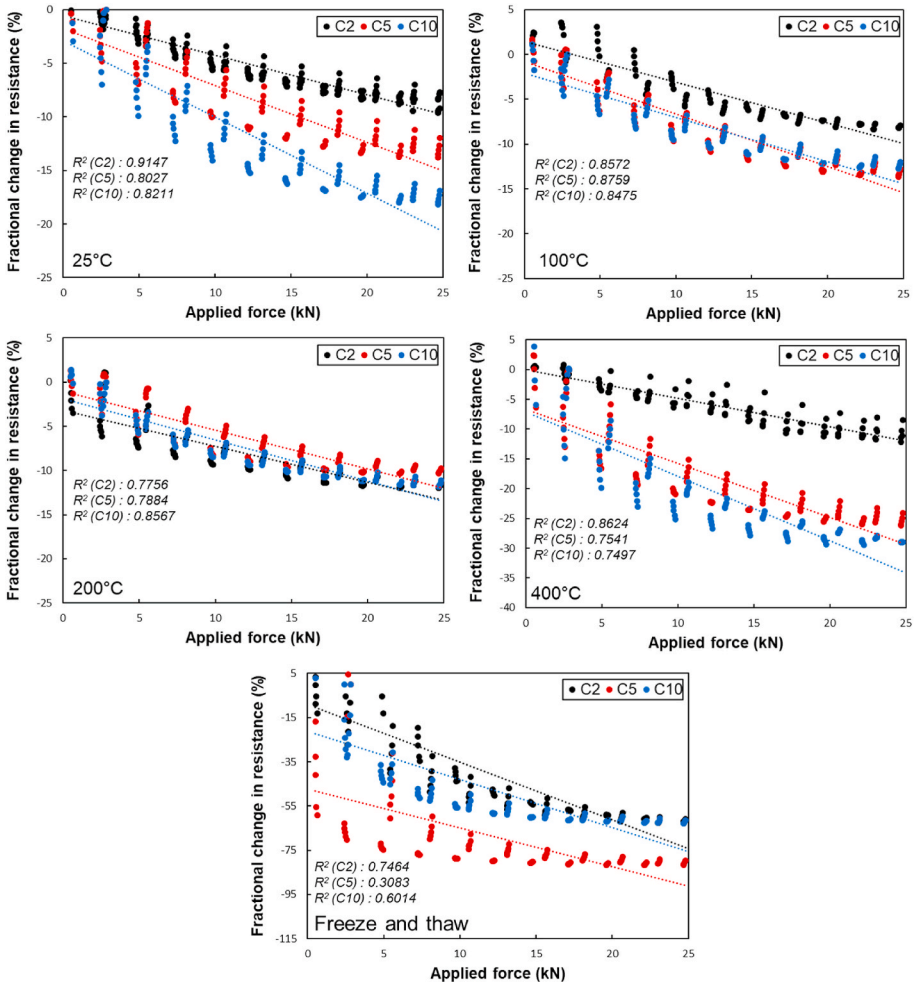

Fig. 5. Fractional change in electrical resistance of the specimens exposed to different temperatures during cyclic loading tests.

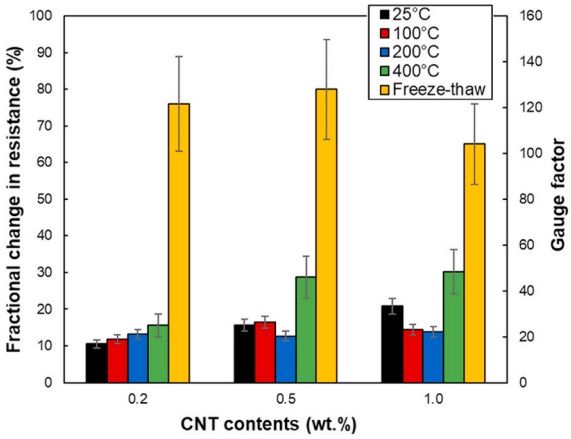

Fig. 6. Fractional change in resistance and gauge factor of the specimens.

melting process of the water [31]. The aim of the present study is to investigate the effects of micro-structural changes in cementitious composites on conductivity and piezoresistivity as the cement-based sensors; thus, elevated temperatures and freeze-thaw cycles were simultaneously considered as experimental conditions in the present study.

3.1. Electrical resistance and compressive strength

The zeta potential values were measured to investigate the dispersion state of the utilized MWCNTs, and the measured values of solutions, including water, MWCNT, and PSS, are listed in Table 3. The zeta potential value of water was −16.9 mV, while that of water with MWCNT and PSS was −10.43 and −26.55 mV, respectively. These values can be calculated as relative values; consequently, the values for water, MWCNT, and PSS will become 0, 6.47, and −9.65 mV, respectively. These results indicate that the MWCNT particles were positively charged, whereas the PSS particles were negatively charged in water [22]. Hence, it is evident that the PSS particles cause the MWCNT particles to adhere to them because they have contrasting zeta potential values. The relative zeta potential value of the solution, including water, MWCNT, and PSS, was −4.32 mV, which is the average value of MWCNT and PSS in water; this indicates that by incorporating PSS, the Van der Waals force between the MWCNT particles can be potentially reduced. Consequently, PSS incorporation can improve the dispersion of MWCNT particles in the specimens, resulting in lower electrical resistance levels, as shown in Fig. 1 (a), compared to those in previous studies [10–12].

The effects of exposure temperatures on the electrical resistance and compressive strength of the cement-based sensors are shown in Fig. 1. The electrical resistance of sensors exposed to a temperature of 100 and 200 °C was similar to that of sensors at 25 °C; however, the electrical resistance of sensors exposed to 400 °C or those subjected to freeze-thaw cycles increased dramatically. As reported in previous studies, the components of the cementitious composites were not completely decomposed upon exposure to 200 °C, which may explain the electrical resistance and compressive strength levels of the cementitious composites [14,23]. However, the components in the cementitious composites started to decompose upon exposure to 400 °C; consequently, the electrical resistance dramatically increased and the compressive strength of the cement-based sensors decreased [14,23]. In addition, the sensors became damaged during the freeze-thaw cycles, leading to porosity [31,32]. Hence, the aforementioned phenomena justify the increased electrical resistance and decreased compressive strength levels.

3.2. Tunneling-induced electrical stability

The tunneling-induced electrical resistance outcomes of the specimens are shown in Fig. 2. Previous studies reported that the tunneling-induced electrical properties of cement-based composites refer to the tunneling effect on the electrical resistance, which usually decreases over time given that electrical conductive networks composed of MWCNTs can be gradually developed [33,34]. Accordingly, the reduction in the electrical resistance of the fabricated cement-based sensors, regardless of the embedded MWCNT content, was noted, as shown in Fig. 2. It was also found that the degree of reduction in electrical resistance was different based on the embedded MWCNT content. A substantial tunneling effect was observed in sensors with low levels of MWCNT, which can be attributed to the fact that the tunneling effect is inversely proportional to the embedded MWCNT content [35,36]. In addition, the tunneling-induced electrical stability of the sensors decreased when they were exposed to temperatures of 100, 200, and 400 °C. This can be explained by the decomposition of components in the cementitious composites, which may disturb the movement of electron charges and reduce the tunneling-induced electrical stability [35]. The sensors subjected to freeze-thaw cycles specifically demonstrated the lowest tunneling-induced electrical stability; this can be confirmed by the appearance of microcracks in the cement-based sensors during the freeze–thaw cycles. The temperature-dependent electrical resistance of sensors during the freeze-thaw cycle tests are shown in Fig. 3. It can be observed that the electrical resistance was inversely proportional to the temperature. As reported in previous studies, the activation energy for electrical conduction increased, possibly leading to a decrease in the electrical resistance of the cement-based sensors as they were heated, indicating a negative temperature coefficient [5,32,35,37]. Similarly, the electrical resistance of the cement-based sensors increased as the temperature was decreased owing to the activation energy of electrical conduc-

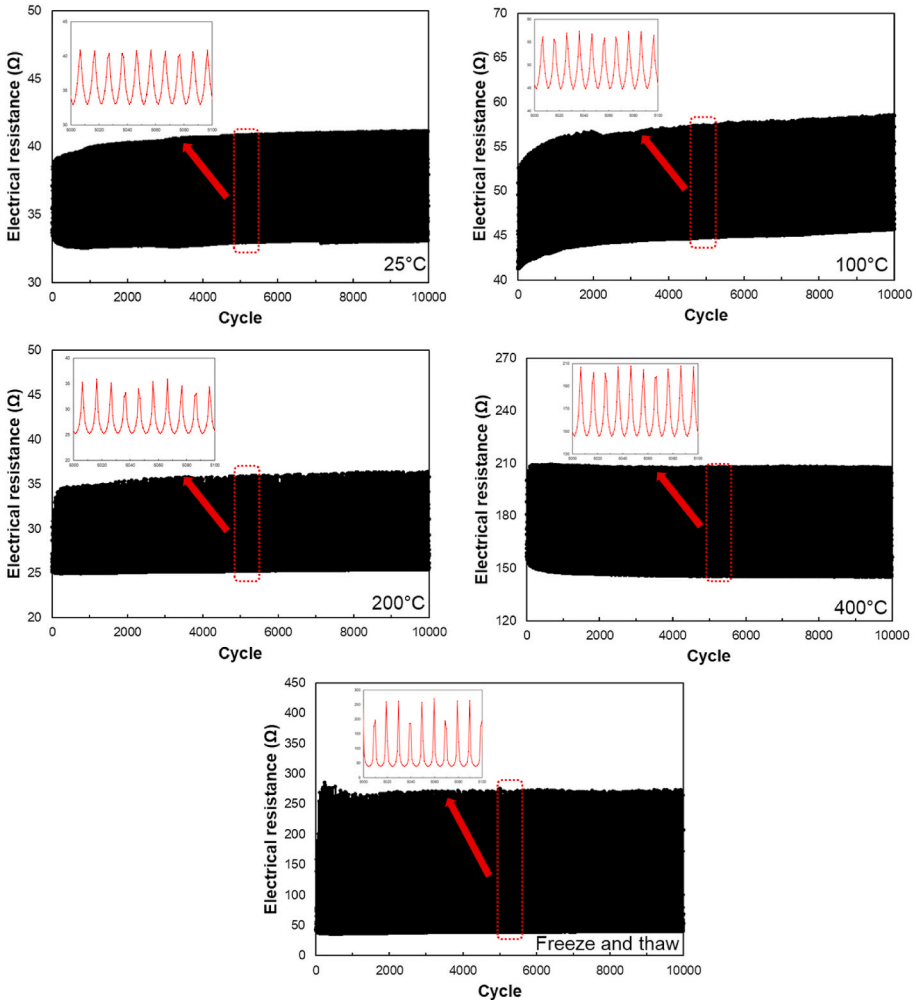

Fig. 7. Electrical resistance of C5 specimen after it was exposed to various temperatures during a loading test of 10,000 cycles.

tion, indicating a positive temperature coefficient. These results are in good agreement with those reported in previous studies [5,32,35,37].

Fig. 3 illustrates the different trends in the sensors based on the embedded MWCNT content. The C5 and C10 specimens showed stable variation of electrical resistance during the freeze and thaw cycles, while the electrical resistance of C2 sensor decreased during the cycling process. These results are supported by the results of tunneling-induced electrical resistance (shown in Fig. 2). The C2 sensor demonstrated a substantial tunneling effect, which can decrease the electrical resistance, while C5 and C10 sensors with a weaker tunneling effect showed stable values during the freeze and thaw cycles.

3.3. *Piezoresistivity performances*

The piezoresistive sensing performance of the fabricated cement-based sensors was investigated using the experimental setup described in Fig. 4, and these results are shown in Fig. 5. In Fig. 5, it can be observed that the electrical resistance of the sensors decreased as the loadings were applied, whereas these capabilities increased as the sensors were unloaded. These phenomena can be explained by the piezoresistive sensing mechanisms; individual MWCNT particles became closer with the application of load, thereby forming electrically conductive pathways comprising MWCNTs and decreasing the electrical resistance [11]. Meanwhile, the sensors exposed to various temperatures developed disturbances in the electrically conductive pathways, thus decreasing the stability of electrical resistance during the cyclic loading process. The linearity expressed as R-squared (R^2) values of the sensors as exposed to different temperatures was observed in Fig. 5. The decreased R^2 values can be seen in the sensors as exposed to 200 and 400 °C. The conductive path ways were disturbed as they were exposed to high temperatures due to the evaporation of moisture and decomposition of hydrates in the cementitious composites, leading to lower linearity and repetability. Meanwhile, it can be noted that the C10 sensor showed comparable higher R^2 value than that of C2 and C5 sensors as they were exposed to 200 °C. This result can be attributed to the formation of conductive path ways and the percolation threshold of cement-based sensors. As reported in previous studies, the percolation threshold of MWCNT-embedded cement-based sensors is in the range of 0.3–0.4% of the embedded MWCNT content based on

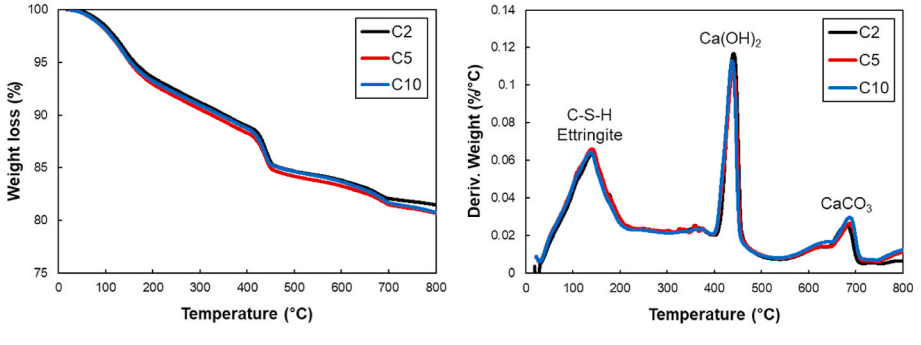

(a)

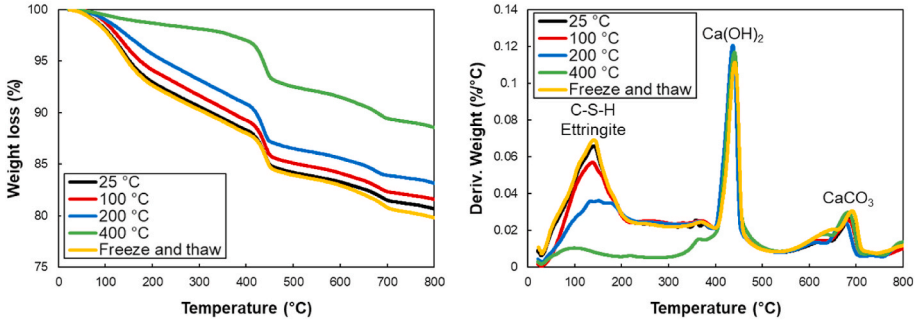

(b)

Fig. 8. TG and DTG results of the specimens with (a) different MWCNT content and (b) and when exposed to various temperatures.

the binder mass [38–40]. Therefore, comparable sparse conductive networks were formed in C2 and C5 sensors, whereas dense networks were formed in and C10; thus, the linearity was not significantly affected in C10 sensor compared to that in C2 and C5 sensors. Although the high R^2 value is observed in the C2 sensor exposed to 400 °C, it can be deduced from the lower sensitivity (i.e., approximately 5% of fractional change in electrical resistance) which causes a high R^2 value.

In addition, the R^2 values decreased dramatically when the sensors were exposed to freeze-thaw cycles. After freeze-thaw cycle, the micro cracks can be formed in the composites due to the freezing and melting process of water. For these reasons, the lower R^2 values (i.e., 0.7464, 0.3083, and 0.6014) were seen in the specimens after the freeze-thaw cycles. Accordingly, it can be concluded that MWCNT-embedded cement-based sensors in which the MWCNT content level exceeds the percolation threshold have high durability under exposure to various temperatures, and it is recommended to include different types of conductive fillers such as carbon fiber and carbon black to mitigate the disconnection of MWCNT-based conductive path ways when the sensors are exposed to freeze and thaw conditions.

Based on the experimental data, the maximum fractional change in the electrical resistance and GF were calculated, as shown in Fig. 6. Higher values of FCR and GF were observed in the sensors after the freeze and thaw cyclic tests, which can be explained by the damage and porosity incurred in the sensors during these tests. The FCR and GF determined in this study demonstrated high stability and sensitivity in comparison to those in previous studies [41].

The stability of the piezoresistive sensing performance of the cement-based sensors in the long-term loading conditions was investigated, as shown in Fig. 7. According to the piezoresistive sensing performance presented in Figs. 5 and 6, sensor C5, which was exposed to various temperatures, was selected for the long-term loading test. Fig. 7 shows that the electrical resistance values of these sensors are stable, thereby demonstrating that the long-term piezoresistive sensing performance is highly stable. In addition, similar fractional resistance changes were noted in the long-term loading conditions, indicating stable sensitivity in sensor C5.

3.4. Physicochemical investigations

The TG and DTG analysis results of the fractured specimens are shown in Fig. 8. It can be observed that the results had three notable DTG peaks in the temperature range of 150–180 °C, 400–450 °C, and 650–700 °C. The first peak in the temperature range of 150–180 °C can be attributed to the dehydration of C–S–H and ettringite, and the AFm phase [42,43]. In addition, the second and third peaks observed at 400–450 °C and 650–700 °C can be explained by the de-hydroxylation and de-carbonation of calcium hydroxide and calcium carbonate, respectively, which are significantly consistent with previous studies [42–45]. It was also observed that the effect of MWCNT content on the loss in weight was negligible, as demonstrated in Fig. 8 (a). This can be attributed to the relative dose of embedded MWCNT content ($\leq$ 1 wt%), which had insignificant effects. Furthermore, it can be known that the MWCNTs are

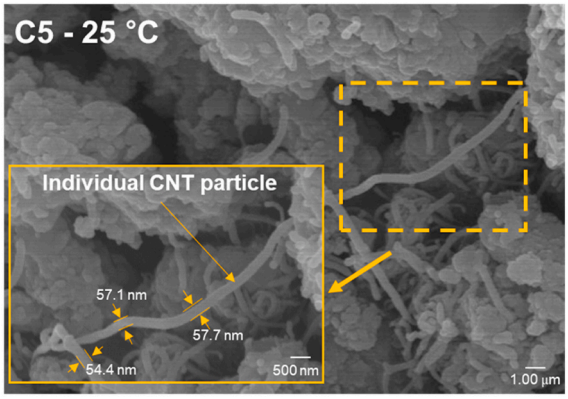

(a)

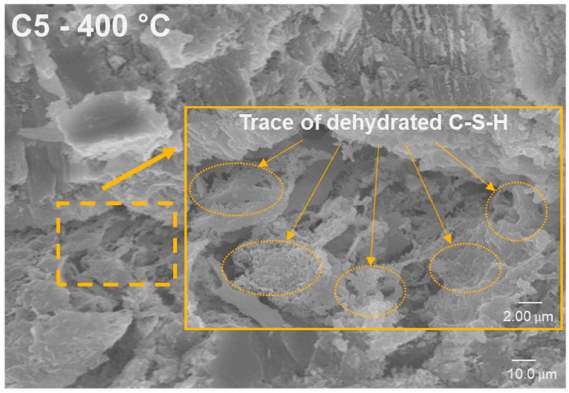

(b)

Fig. 9. SEM images of C5 specimen exposed to different temperatures.

decomposed in the exposure temperature range between 450 °C and 700 °C [46–48]. Considering the decomposition temperature of MWCNTs, it can be concluded that the effects of exposure temperature (≤ 400 °C) on the electrical conductivity of the specimens are mainly affected by the de-hydrate of C–S–H and ettringite [14].

The exposure temperatures of the cement-based sensors significantly impacted the TG and DTG results (see Fig. 8 (b)). The fractured specimens of cement-based sensors exposed to temperatures of 100, 200, and 400 °C exhibited less weight loss compared to those exposed to 25 °C and those that were subjected to freeze-thaw conditions; specimens exposed to temperatures of 25, 100, 200, and 400 °C, and freeze-thaw cycles experienced a weight loss of 5.96, 4.86, 3.38, 1.15, and 6.34%, respectively. These results likely stem from the dehydration of C–S–H in the exposure conditions. Additionally, Fig. 9 presents the SEM images of the electrically conductive pathways in sensor C5. Individual MWCNT particles were observed in the sensor exposed to 25 °C; however, the trace of dehydrated C–S–H disturbed the formation of conductive pathways in this case. This hypothesis can be explained by the TG results shown in Fig. 8 (a). It can be known that the main feature of TG result in the temperature range between 100 °C and 400 °C is the C–S–H and ettringite, and the specimens exposed to elevated temperature (i.e., 200 °C and 400 °C) showed the lower weight loss (Fig. 8 (b)). Thus, it can be said that the de-hydrate of C–S–H and ettringite shown in SEM image is the dominant factor which affect the electrical properties of the specimens, and it can hinder the connection of MWCNT particles, increasing the electrical resistances. For these reasons, the authors can conclude that the sensors exposed to 200 °C and 400 °C with dehydrated C–S–H and ettringite likely had increased electrical resistances, an outcome in close agreement with the results shown in Fig. 1.

4. Conclusions

In this study, cement-based sensors incorporating various MWCNT content were fabricated, and their electrical, piezoresistive sensing, and physicochemical characteristics, exposed to various temperatures, were investigated. The sensors were exposed to five different temperatures, and their electrical characteristics and piezoresistive sensing performance were examined under two different dynamic loading conditions. The test results were discussed in terms of the results of TG/DTG and FE-SEM analyses; the key findings of this study are presented below:

1) The effects of exposure temperatures on the electrical characteristics of cement-based sensors were investigated. C–S–H dehydration occurred when the sensors were exposed to elevated temperatures because the formation of electrically conductive pathways comprising MWCNTs was disturbed, leading to a significant decrease in electrical conductivity.
2) The tunneling-induced and temperature-dependent electrical resistance of the sensors was observed. The sensors with MWCNT content exceeding the percolation threshold ($\geq$ 0.4 wt%) showed higher stability for tunneling-induced and temperature-dependent electrical properties in comparison to those with MWCNT content less than the percolation threshold.
3) The piezoresistive sensing performance of the sensors was affected by the exposure temperature. Specifically, the cement-based sensors with relatively low MWCNT content were significantly affected by the exposure temperature. However, the sensors with MWCNT content exceeding the percolation threshold range showed greater stability for the piezoresistive sensing performance in both short- and long-term loading conditions.

Credit author statement

Daeik Jang: Writing – original draft, Conceptualization, Methodology; **H. N. Yoon**: Data curation, Investigation; **Joonho Seo**: Methodology, Formal analysis, Validation; **Beomjoo Yang**: Writing – review and editing, Supervision.

Declaration of competing interest

The authors declare that they have no known competing financial interests or personal relationships that could have appeared to influence the work reported in this paper.

Acknowledgment

This work was supported by the National Research Foundation of Korea grant funded by the Korean government (MSIT) (2020R1C1C1005063).

References

[1] B. Han, X. Yu, E. Kwon, A self-sensing carbon nanotube/cement composite for traffic monitoring, Nanotechnology 20 (2009) 445501, https://doi.org/10.1088/0957-4484/20/44/445501.
[2] B. Han, K. Zhang, X. Yu, E. Kwon, J. Ou, Electrical characteristics and pressure-sensitive response measurements of carboxyl MWNT/cement composites, Cement Concr. Compos. 34 (2012) 794–800, https://doi.org/10.1016/j.cemconcomp.2012.02.012.
[3] G.M. Kim, I.W. Nam, B. Yang, H.N. Yoon, H.K. Lee, S. Park, Carbon nanotube (CNT) incorporated cementitious composites for functional construction materials: the state of the art, Compos. Struct. 227 (2019) 111244, https://doi.org/10.1016/j.compstruct.2019.111244.
[4] D.I. Jang, G.E. Yun, J.E. Park, Y.K. Kim, Designing an attachable and power-efficient all-in-one module of a tunable vibration absorber based on magnetorheological elastomer, Smart Mater. Struct. 27 (2018) 85009, https://doi.org/10.1088/1361-665X/aacdbd.
[5] D. Jang, H.N. Yoon, J. Seo, H.K. Lee, G.M. Kim, Effects of silica aerogel inclusion on the stability of heat generation and heat-dependent electrical characteristics of cementitious composites with CNT, Cement Concr. Compos. 115 (2021) 103861, https://doi.org/10.1016/j.cemconcomp.2020.103861.
[6] H.N. Yoon, D. Jang, H.K. Lee, I.W. Nam, Influence of carbon fiber additions on the electromagnetic wave shielding characteristics of CNT-cement composites, Construct. Build. Mater. (2020) 121238, https://doi.org/10.1016/j.conbuildmat.2020.121238.
[7] D.I. Jang, H.N. Yoon, I.W. Nam, H.K. Lee, Effect of carbonyl iron powder incorporation on the piezoresistive sensing characteristics of CNT-based polymeric sensor, Compos. Struct. 244 (2020) 112260, https://doi.org/10.1016/j.compstruct.2020.112260.
[8] Y.-K. Kim, J. Kim, D. Jang, S. Kim, W. Jung, A study on the effects of multiwall carbon nanotubes on dynamic stiffness of hydrophilic-base magnetorheological gel, Curr. Nanosci. 15 (2018) 319–323, https://doi.org/10.2174/1573413714666181023144334.
[9] L. Zhang, S. Ding, L. Li, S. Dong, D. Wang, X. Yu, B. Han, Effect of characteristics of assembly unit of CNT/NCB composite fillers on properties of smart cement-based materials, Compos. Part A Appl. Sci. Manuf. 109 (2018) 303–320, https://doi.org/10.1016/j.compositesa.2018.03.020.
[10] F. Naeem, H.K. Lee, H.K. Kim, I.W. Nam, Flexural stress and crack sensing capabilities of MWNT/cement composites, Compos. Struct. 175 (2017) 86–100, https://doi.org/10.1016/j.compstruct.2017.04.078.
[11] I.W. Nam, H. Souri, H.K. Lee, Percolation threshold and piezoresistive response of multi-wall carbon nanotube/cement composites, Smart Struct. Syst. 18 (2016) 217–231, https://doi.org/10.12989/sss.2016.18.2.217.
[12] H.K. Kim, I.S. Park, H.K. Lee, Improved piezoresistive sensitivity and stability of CNT/cement mortar composites with low water-binder ratio, Compos. Struct. 116 (2014) 713–719, https://doi.org/10.1016/j.compstruct.2014.06.007.
[13] Y. Wang, X. Zhao, Y. Zhao, Piezoresistivity of cement matrix composites incorporating multiwalled carbon nanotubes due to moisture variation, Adv. Civ. Eng. 2020 (2020), https://doi.org/10.1155/2020/5476092.
[14] W. Dong, W. Li, K. Wang, B. Han, D. Sheng, S.P. Shah, Investigation on physicochemical and piezoresistive properties of smart MWCNT/cementitious composite exposed to elevated temperatures, Cement Concr. Compos. 112 (2020) 103675, https://doi.org/10.1016/j.cemconcomp.2020.103675.
[15] D. Jang, H.N. Yoon, S.Z. Farooq, H.K. Lee, I.W. Nam, Influence of water ingress on the electrical properties and electromechanical sensing capabilities of CNT/cement composites, J. Build. Eng. 42 (2021) 103065, https://doi.org/10.1016/j.jobe.2021.103065.
[16] M.J. Lim, H.K. Lee, I.W. Nam, H.K. Kim, Carbon nanotube/cement composites for crack monitoring of concrete structures, Compos. Struct. 180 (2017) 741–750, https://doi.org/10.1016/j.compstruct.2017.08.042.
[17] H.K. Lee, I.W. Nam, M. Tafesse, H.K. Kim, Fluctuation of electrical properties of carbon-based nanomaterials/cement composites: case studies and parametric modeling, Cement Concr. Compos. 102 (2019) 55–70, https://doi.org/10.1016/j.cemconcomp.2019.04.008.
[18] M. Tafesse, N. Kon, A. Shiferaw, H. Kyoung, S. Wook, H. Kim, Flowability and electrical properties of cement composites with mechanical dispersion of carbon nanotube, Construct. Build. Mater. 293 (2021) 123436, https://doi.org/10.1016/j.conbuildmat.2021.123436.
[19] E. García-Macías, A. Downey, A. D'Alessandro, R. Castro-Triguero, S. Laflamme, F. Ubertini, Enhanced lumped circuit model for smart nanocomposite cement-based sensors under dynamic compressive loading conditions, Sensors Actuators, A Phys. 260 (2017) 45–57, https://doi.org/10.1016/j.sna.2017.04.004.
[20] H. Sun, Z. Ren, S.A. Memon, D. Zhao, X. Zhang, D. Li, F. Xing, Investigating drying behavior of cement mortar through electrochemical impedance spectroscopy analysis, Construct. Build. Mater. 135 (2017) 361–368, https://doi.org/10.1016/j.conbuildmat.2016.12.196.
[21] H.K. Kim, I.W. Nam, H.K. Lee, Enhanced effect of carbon nanotube on mechanical and electrical properties of cement composites by incorporation of silica fume, Compos. Struct. 107 (2014) 60–69, https://doi.org/10.1016/j.compstruct.2013.07.042.
[22] G.M. Kim, T. Kil, H.K. Lee, A novel physicomechanical approach to dispersion of carbon nanotubes in polypropylene composites, Compos. Struct. 258 (2020) 113377, https://doi.org/10.1016/j.compstruct.2020.113377.
[23] J. Seo, S.J. Bae, D.I. Jang, S. Park, B. Yang, H.K. Lee, Thermal behavior of alkali-activated fly ash/slag with the addition of an aerogel as an aggregate replacement, Cement Concr. Compos. 106 (2020) 103462, https://doi.org/10.1016/j.cemconcomp.2019.103462.

[24] H.R. Khalid, I. Choudhry, D. Jang, N. Abbas, M.S. Haider, H.K. Lee, Facile synthesis of sprayed CNTs layer-embedded stretchable sensors with controllable sensitivity, Polymers 13 (2021) 1–6, https://doi.org/10.3390/polym13020311.
[25] J.E. Park, G.E. Yun, D.I. Jang, Y.K. Kim, Analysis of electrical resistance and impedance change of magnetorheological gels with DC and AC voltage for magnetometer application, Sensors (2019) 19, https://doi.org/10.3390/s19112510.
[26] W.S. Bao, S.A. Meguid, Z.H. Zhu, G.J. Weng, Tunneling resistance and its effect on the electrical conductivity of carbon nanotube nanocomposites, J. Appl. Phys. 111 (2012), https://doi.org/10.1063/1.4716010.
[27] G.M. Kim, S.M. Park, G.U. Ryu, H.K. Lee, Electrical characteristics of hierarchical conductive pathways in cementitious composites incorporating CNT and carbon fiber, Cement Concr. Compos. 82 (2017) 165–175, https://doi.org/10.1016/j.cemconcomp.2017.06.004.
[28] B.H. Manan Bhandari, Jianchao Wang, Daeik Jang, llWoo Nam, A comparative study on the electrical and piezoresistive sensing characteristics of GFRP and CFRP composites with hybridized incorporation of carbon nanotubes, graphenes, carbon nanofibers, and graphite nanoplatelets, Sensors 21 (2021) 7291, https://doi.org/10.3390/s21217291.
[29] R. Snellings, J. Chwast, Ö. Cizer, N. De Belie, Y. Dhandapani, P. Durdzinski, J. Elsen, J. Haufe, D. Hooton, C. Patapy, M. Santhanam, K. Scrivener, D. Snoeck, L. Steger, S. Tongbo, A. Vollpracht, F. Winnefeld, B. Lothenbach, RILEM TC-238 SCM recommendation on hydration stoppage by solvent exchange for the study of hydrate assemblages, Mater. Struct. Constr. 51 (2018), https://doi.org/10.1617/s11527-018-1298-5.
[30] S.J. Bae, S. Park, H.K. Lee, Role of Al in the crystal growth of alkali-activated fly ash and slag under a hydrothermal condition, Construct. Build. Mater. 239 (2020) 117842, https://doi.org/10.1016/j.conbuildmat.2019.117842.
[31] H. Wu, Z. Liu, B. Sun, J. Yin, Experimental investigation on freeze-thaw durability of Portland cement pervious concrete (PCPC), Construct. Build. Mater. 117 (2016) 63–71, https://doi.org/10.1016/j.conbuildmat.2016.04.130.
[32] J. Cao, D.D.L. Chung, Damage evolution during freeze-thaw cycling of cement mortar, studied by electrical resistivity measurement, Cement Concr. Res. 32 (2002) 1657–1661, https://doi.org/10.1016/S0008-8846(02)00856-6.
[33] Y. Wang, G.J. Weng, S.A. Meguid, A.M. Hamouda, A continuum model with a percolation threshold and tunneling-assisted interfacial conductivity for carbon nanotube-based nanocomposites, J. Appl. Phys. 115 (2014), https://doi.org/10.1063/1.4878195.
[34] N. Hu, Y. Karube, C. Yan, Z. Masuda, H. Fukunaga, Tunneling effect in a polymer/carbon nanotube nanocomposite strain sensor, Acta Mater. 56 (2008) 2929–2936, https://doi.org/10.1016/j.actamat.2008.02.030.
[35] G.M. Kim, B.J. Yang, H.N. Yoon, H.K. Lee, Synergistic effects of carbon nanotube and carbon fiber on heat generation and electrical characteristics of cementitious composites, Carbon N. Y. 134 (2018) 283–292, https://doi.org/10.1016/j.carbon.2018.03.070.
[36] Z. Xiang, T. Chen, Z. Li, X. Bian, Negative Temperature Coefficient of Resistivity in Lightweight Conductive Carbon Nanotube/Polymer Composites, 2009, pp. 91–95, https://doi.org/10.1002/mame.200800273.
[37] G.M. Kim, F. Naeem, H.K. Kim, H.K. Lee, Heating and heat-dependent mechanical characteristics of CNT-embedded cementitious composites, Compos. Struct. 136 (2016) 162–170, https://doi.org/10.1016/j.compstruct.2015.10.010.
[38] B. Han, X. Yu, E. Kwon, J. Ou, Effects of CNT concentration level and water/cement ratio on the piezoresistivity of CNT/cement composites, J. Compos. Mater. 46 (2012) 19–25, https://doi.org/10.1177/0021998311401114.
[39] I.W. Nam, H.K. Lee, J.B. Sim, S.M. Choi, Electromagnetic characteristics of cement matrix materials with carbon nanotubes, ACI Mater. J. 109 (2012) 363–370, https://doi.org/10.14359/51683827.
[40] I.W. Nam, H.K. Lee, Image analysis and DC conductivity measurement for the evaluation of carbon nanotube distribution in cement matrix, Int. J. Concr. Struct. Mater. 9 (2015) 427–438, https://doi.org/10.1007/s40069-015-0121-8.
[41] Q. Liu, R. Gao, V.W.Y. Tam, W. Li, J. Xiao, Strain monitoring for a bending concrete beam by using piezoresistive cement-based sensors, Construct. Build. Mater. 167 (2018) 338–347, https://doi.org/10.1016/j.conbuildmat.2018.02.048.
[42] J. Seo, S. Park, H.N. Yoon, H.K. Lee, Effect of CaO incorporation on the microstructure and autogenous shrinkage of ternary blend Portland cement-slag-silica fume, Construct. Build. Mater. 249 (2020) 118691, https://doi.org/10.1016/j.conbuildmat.2020.118691.
[43] H.N. Yoon, J. Seo, S. Kim, H.K. Lee, S. Park, Hydration of calcium sulfoaluminate cement blended with blast-furnace slag, Construct. Build. Mater. 268 (2021) 121214, https://doi.org/10.1016/j.conbuildmat.2020.121214.
[44] H.N. Yoon, J. Seo, S. Kim, H.K. Lee, S. Park, Characterization of blast furnace slag-blended Portland cement for immobilization of Co, Cement Concr. Res. 134 (2020) 106089, https://doi.org/10.1016/j.cemconres.2020.106089.
[45] O.P. Kari, Y. Elakneswaran, T. Nawa, J. Puttonen, A model for a long-term diffusion of multispecies in concrete based on ion-cement-hydrate interaction, J. Mater. Sci. 48 (2013) 4243–4259, https://doi.org/10.1007/s10853-013-7239-3.
[46] C.M. Chen, M. Chen, F.C. Leu, S.Y. Hsu, S.C. Wang, S.C. Shi, C.F. Chen, Purification of multi-walled carbon nanotubes by microwave digestion method, Diam. Relat. Mater. 13 (2004) 1182–1186, https://doi.org/10.1016/j.diamond.2003.11.016.
[47] J. He, J. Chen, L. Shi, Q. Li, W. Lu, S. Qu, W. Qiu, G. Zhou, Fabrication of thermally robust carbon nanotube (CNT)/SiO 2 composite films and their high-temperature mechanical properties, Carbon N. Y. 147 (2019) 236–241, https://doi.org/10.1016/j.carbon.2019.02.088.
[48] T. Arunkumar, R. Karthikeyan, R. Ram Subramani, K. Viswanathan, M. Anish, Synthesis and characterisation of multi-walled carbon nanotubes (MWCNTs), Int. J. Ambient Energy 41 (2020) 452–456, https://doi.org/10.1080/01430750.2018.1472657.